

Novel Magnetic Block States in Low-Dimensional Iron-Based Superconductors

J. Herbrych^{1,2}, J. Heverhagen^{3,4}, N. D. Patel⁵, G. Alvarez⁶, M. Daghofer^{3,4}, A. Moreo^{1,2}, and E. Dagotto^{1,2}

¹ *Department of Physics and Astronomy, University of Tennessee, Knoxville, Tennessee 37996, USA*

² *Materials Science and Technology Division, Oak Ridge National Laboratory, Oak Ridge, Tennessee 37831, USA*

³ *Institute for Functional Matter and Quantum Technologies, University of Stuttgart, Pfaffenwaldring 57, D-70550 Stuttgart, Germany*

⁴ *Center for Integrated Quantum Science and Technology, University of Stuttgart, Pfaffenwaldring 57, D-70550 Stuttgart, Germany*

⁵ *Department of Physics, Ohio State University, Columbus, Ohio 43210, USA and*

⁶ *Computational Sciences and Engineering Division and Center for Nanophase Materials Sciences, Oak Ridge National Laboratory, Oak Ridge, Tennessee 37831, USA*

(Dated: December 4, 2018)

Inelastic neutron scattering (INS) has recently confirmed the existence of an antiferromagnetic $\uparrow\uparrow\downarrow\downarrow$ -pattern along the legs of quasi-one dimensional iron-based ladders, as predicted for the orbital-selective Mott phase (OSMP) of multi-orbital systems. We show here that electron-doping of the OSMP induces a whole class of novel block-states with a variety of periodicities beyond the previously reported $\pi/2$ pattern. We discuss the magnetic phase diagram of the OSMP regime that could be tested by INS employing samples at the appropriate dopings.

Introduction. It is well established that competing energy scales and interactions in strongly correlated electronic systems can induce novel and exotic effects. A clear example are the iron-based superconductors [1–4] where charge, spin, orbital, and lattice degrees of freedom combine phenomena known from cuprates with those found in manganites. Prominent among these novel effects is the orbital-selective Mott phase (OSMP) [5]. In this regime, electron-electron interactions acting on a multi-orbital Fermi surface with several pockets cause the selective localization of electrons on one of the orbitals. As a consequence, the system is in a state with coexisting metallic and Mott-insulating bands [see Fig. 1(a)].

The OSMP was proven to be relevant for a class of quasi-one-dimensional (quasi-1D) iron-based materials of the 123 family [6–8] (AFe_2X_3 ; A alkali metals, X=Se,S chalcogenides). Recent theoretical investigations [9, 10] and inelastic neutron scattering (INS) experiments [8] unveiled the existence of a $\pi/2$ -block magnetic state where spins form antiferromagnetically (AFM) coupled ferromagnetic (FM) islands, in a $\uparrow\uparrow\downarrow\downarrow$ -pattern [see Fig. 1(b)]. This unusual spin-block state was observed in BaFe_2Se_3 [8]. Similar patterns in two-dimensional systems with iron vacancies, such as $\text{Rb}_{0.89}\text{Fe}_{1.58}\text{Se}_2$ [11] and $\text{K}_{0.8}\text{Fe}_{1.6}\text{Se}_2$ [12–15], were also reported before.

In this Letter we will show that (i) electron-doping of the block-OSMP could actually lead to a whole new class of spin states, beyond the previously reported $\pi/2$ -pattern. Such block-states come in various shapes and sizes depending on filling and lattice geometry. Also, (ii) we will develop an effective Hamiltonian for the OSMP. Our results have various consequences: (iii) they allow for an intuitive understanding of the origin of the block magnetism in multi-orbital systems and (iv) provide a simple model for accurate OSMP numerical investigations. Furthermore, (v) we predict the behavior of the maximum of the spin structure factor in electron-

doped materials which can be tested by INS studies.

Model. Our conclusions are based on extensive simulations of two- and three-orbital models in chain and ladder geometries for a variety of model parameters, see Supplementary Material [16]. We first focus for clarity on the two-orbital 1D Hubbard model defined as,

$$H_{\text{H}} = - \sum_{\gamma, \gamma', \ell, \sigma} t_{\gamma\gamma'} \left(c_{\gamma, \ell, \sigma}^\dagger c_{\gamma', \ell+1, \sigma} + \text{H.c.} \right) + \Delta \sum_{\ell} n_{1, \ell} + U \sum_{\gamma, \ell} n_{\gamma, \ell, \uparrow} n_{\gamma, \ell, \downarrow} + (U - 5J_{\text{H}}/2) \sum_{\ell} n_{0, \ell} n_{1, \ell} - 2J_{\text{H}} \sum_{\ell} \mathbf{S}_{0, \ell} \cdot \mathbf{S}_{1, \ell} + J_{\text{H}} \sum_{\ell} \left(P_{0, \ell}^\dagger P_{1, \ell} + \text{H.c.} \right), \quad (1)$$

where $c_{\gamma, \ell, \sigma}^\dagger$ creates an electron with spin $\sigma = \{\uparrow, \downarrow\}$ at orbital $\gamma = \{0, 1\}$ and site $\ell = \{1, \dots, L\}$. $t_{\gamma\gamma'}$ denotes a diagonal hopping amplitude matrix defined in the orbital space γ with $t_{00} = -0.5$ and $t_{11} = -0.15$ in eV units. The crystal-field splitting is $\Delta = 0.8$ eV (kinetic energy bandwidth is $W = 2.1$ eV). The local (γ, ℓ) orbital-resolved particle density is $n_{\gamma, \ell} = \sum_{\sigma} n_{\gamma, \ell, \sigma}$, $\mathbf{S}_{\gamma, \ell}$ is the local spin, and $P_{\gamma, \ell} = c_{\gamma, \ell, \uparrow} c_{\gamma, \ell, \downarrow}$ is the pair-hopping operator. The global filling is $n = N/L$, where N is the number of electrons and L the system size. U is the repulsive Hubbard interaction, while J_{H} stands for the Hund exchange, fixed here to $J_{\text{H}} = U/4$ [17, 18], as in previous publications [9, 10, 19–22]. The Hamiltonians are all diagonalized using the density matrix renormalization group method [23–27] keeping the truncation errors smaller than $\sim 10^{-7}$. Open boundary conditions were assumed.

As long as the system is in the block-OSMP state, our results are *not* sensitive to details of the parameter sets. The same conclusions can be drawn from a system with or without interorbital hybridization and with two or three orbitals. As discussed below, ladder geometries also lead to consistent findings. We also find block states

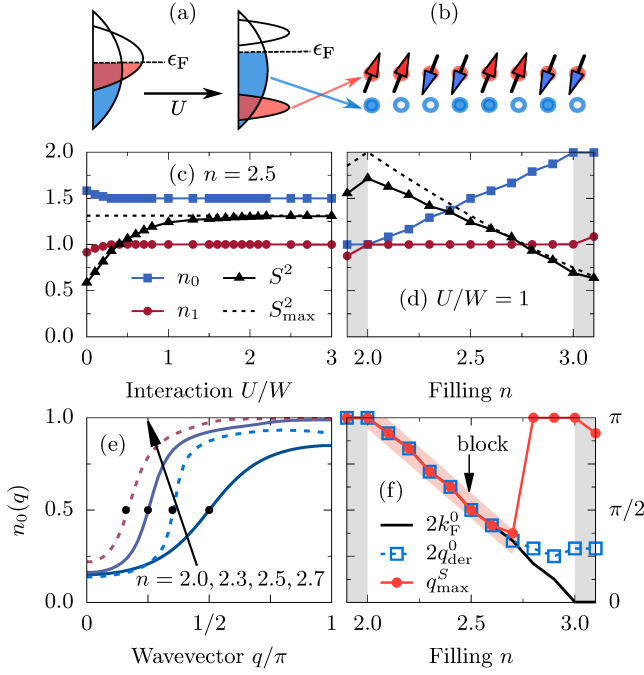


Figure 1. (Color online) Schematic representation of (a) the orbital-selective Mott phase addressed here and (b) the previously known spin block state. (c) Interaction U and (d) filling n dependence of the total magnetic moment $\langle S_\ell^2 \rangle$ and orbital-resolved occupation numbers n_γ of the two-orbital Hubbard model Eq. (1), calculated using $L = 48$ sites. Black dashed lines represent the largest possible magnetic moment S_{\max}^2 . (e) Momentum distribution function $n_0(q)$ of the $\gamma = 0$ orbital. Points indicate q_{der}^0 , i.e. the position of the maximum in $dn_0(q)/dq$. (f) n dependence of the position of the maximum of the spin structure factor q_{\max}^S . Block-OSMP is indicated as a colored area. In the same panel we also present the position of the orbital $\gamma = 0$ Fermi-vector as calculated via $2k_F^0 = \pi n_0$ and position of the maximum of $dn(q)/dq$, i.e. $2q_{\text{der}}^0$.

in the effective Kondo-Heisenberg model. Results are thus generic and intrinsic of multi-orbital systems in the block-OSMP.

Orbital-selective Mott phase. Figures 1(c-d) present the orbital-resolved occupation numbers n_γ and the square of the total magnetic moment per site $\langle S_\ell^2 \rangle = S_\ell(S_\ell + 1)$. As expected in the OSMP, increasing the interaction U “locks” the occupation number of one of the orbitals to $n_1 = 1$. This behavior is observed for all fillings relevant for the OSMP, $2 < n < 3$ region, yielding a remaining orbital $\gamma = 0$ only fractionally occupied. Note that for $n \geq 3$ the latter becomes a band insulator (BI) with $n_0 = 2$. Simultaneously, $\langle S_\ell^2 \rangle$ is almost fully saturated to its maximal value (given by the total filling) when $n_1 = 1$. Charge fluctuations $\delta n_\gamma^2 = \langle n_\gamma^2 \rangle - \langle n_\gamma \rangle^2$ [16, 21] indicate that the number of doublons is highly suppressed on the single-occupied orbital, quite different from the fractionally occupied orbital $\gamma = 0$ where $\delta n_0^2 \neq 0$ shows its metallic character. The results above,

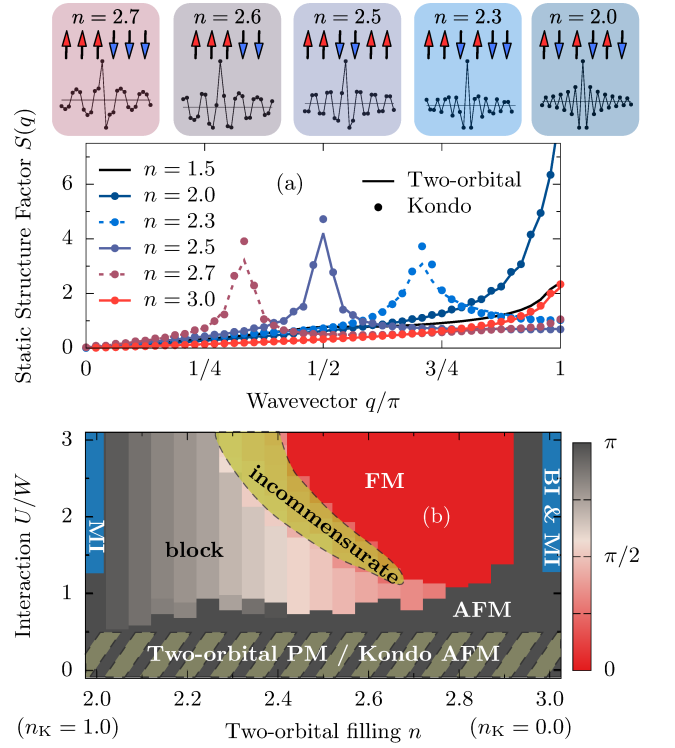


Figure 2. (Color online) (a) Total static structure factor $S(q)$ for various fillings n and fixed $U = W$, for the two-orbital Hubbard model (lines) and the generalized Kondo-Heisenberg model (points), both using $L = 48$ lattice sites. Real-space correlation functions $\langle \mathbf{S}_\ell \cdot \mathbf{S}_{L/2} \rangle$ of the two-orbital Hubbard model and sketches of the spin alignment are also presented at the top. (b) Interaction vs filling magnetic phase diagram obtained with the generalized Kondo-Heisenberg model using $L = 48$ sites. The dashed-shaded region at low- U is where the mapping is not valid.

together with our orbital-resolved density-of-states analysis [16], are consistent with OSMP physics in a wide range $2 < n < 3$.

Block magnetism. Previous efforts showed that the OSMP can have exotic magnetic properties, such as AFM coupled FM islands in the so-called spin-block phase. Readers are referred to Refs. 9 and 10 for a detailed study of the $\pi/2$ -block $\uparrow\uparrow\downarrow\downarrow$ -pattern. Here, one of our main results is that the magnetic pattern of the block-OSMP is *not* limited to this $\pi/2$ -phase, but remarkably the OSMP can support a variety of spin patterns previously unknown. Figure 2(a) illustrates the filling n dependence of the total spin structure factor $S(q) = [2/\pi/(L+1)] \sum_{\ell, m} \exp[iq(\ell - m)] \langle \mathbf{S}_\ell \cdot \mathbf{S}_m \rangle$ [28]. Several conclusions can be obtained directly from the displayed results obtained at $U = W$: (i) below half-filling, $n < 2$, the (weak) maximum of $S(q)$ at $q = \pi$ indicates a paramagnetic state with short-range spin staggered tendencies. (ii) When the system enters the OSMP phase, $2 < n < 3$, we observe quasi-long-range correlations [16] with well-defined peaks in $S(q)$ at q_{\max}^S . In this region

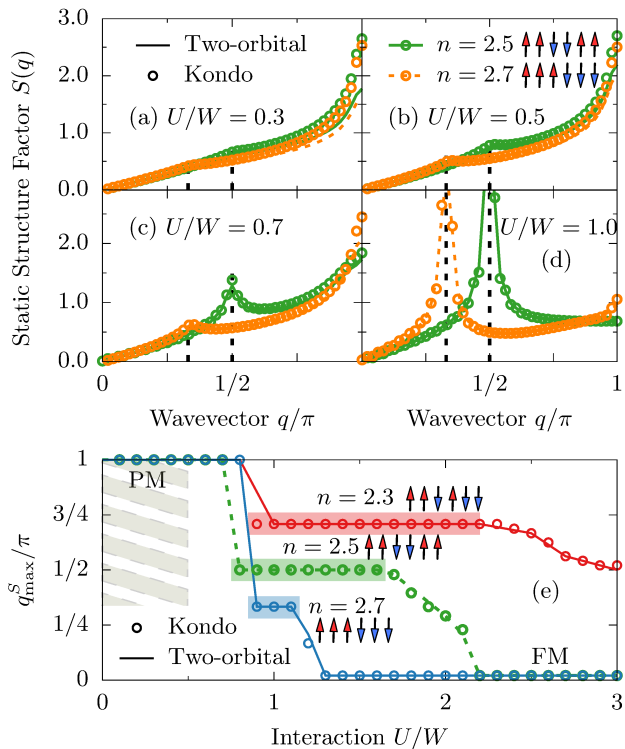


Figure 3. (Color online) (a-d) Interaction U dependence of the total spin structure factor $S(q)$ for $n = 2.5$ and 2.7 . Lines (circles) represent results using the two-orbital Hubbard model (generalized Kondo-Heisenberg model), using $L = 48$ sites. Dashed horizontal lines represent $2k_F = \pi n$. (e) U dependence of q_{\max}^S for the two-orbital Hubbard model (lines) and generalized Kondo-Heisenberg model (circles) at three different fillings $n = 2.3, 2.5$, and 2.7 . Highlighted are the block-OSMP states we found. The dashed-shaded area at low- U represents the region where the mapping is not valid.

q_{\max}^S is strongly dependent on the filling n , and decreases as n increases [see also Fig. 1(f)]. (iii) For $n > 3$ the system again exhibits paramagnetism with a (weak) maximum at $q = \pi$ [29].

Let us focus now on the real-space correlation functions $\langle \mathbf{S}_\ell \cdot \mathbf{S}_{L/2} \rangle$ [Fig. 2(a), top]. Starting with $n = 2$ the structure factor has a “standard” π -AFM staggered spin pattern, common of Mott insulators. However, at $n \simeq 2.3$ an unexpected novel spin pattern emerges involving 1- and 2-sites FM islands of the form $\uparrow\uparrow\downarrow\downarrow$. At $n = 2.5$ the previously known AFM coupled FM blocks of two spins, namely $\uparrow\uparrow\downarrow$, is stabilized. Upon further electron doping the magnetic islands continue growing in size. On the considered lattice of $L = 48$ sites, the largest new pattern observed contains FM blocks with three spins ($\uparrow\uparrow\downarrow\downarrow$) for $n \simeq 2.7$. Increasing n further, $S(q)$ suddenly reaches a maximum again at $q_{\max}^S = \pi$. For a large enough system (not achievable by our method) larger FM islands could be possible, such as containing four spins and beyond [30], albeit likely in narrow regions of parameter space.

Alternatively, at $n = 2.6$ we also identified an exotic $\uparrow\uparrow\downarrow\downarrow\uparrow\uparrow\downarrow\downarrow$ pattern with a long periodicity, showing that even at intermediate n 's, the system still finds a way to stabilize block phases with sharp boundaries, instead of a more smooth “sinusoidal”-like spin pattern.

Effective model. To better understand these surprisingly rich OSMP new magnetic structures, let us consider an effective Hamiltonian. As already discussed, in the OSMP the double occupancy on the localized orbital $\gamma = 1$ with $n_1 = 1$ is highly suppressed. It is therefore natural to restrict - by means of the Schrieffer-Wolff transformation [31] - the Hilbert space of Eq. (1) to the subspace with strictly one electron per site at $\gamma = 1$ orbital. The formal derivation is given in [16], and here we just present the final result, i.e., the generalized Kondo-Heisenberg model defined as,

$$H_K = t_{00} \sum_{\ell, \sigma} \left(c_{0, \ell, \sigma}^\dagger c_{0, \ell+1, \sigma} + \text{H.c.} \right) + U \sum_{\ell} n_{0, \ell, \uparrow} n_{0, \ell, \downarrow} + K \sum_{\ell} \mathbf{S}_{1, \ell} \cdot \mathbf{S}_{1, \ell+1} - J_K \sum_{\ell} \mathbf{S}_{0, \ell} \cdot \mathbf{S}_{1, \ell}, \quad (2)$$

with $K = 4t_{11}^2/U$ and $J_K = 2J_H$. The electronic filling of the effective Hamiltonian is either $n_K = n - 1$ or $n_K = 3 - n$ due to the particle-hole symmetry of Eq. (2). We have tested the accuracy of Eq. (2) by comparing results for $S(q)$ in a wide range of parameters. It is clear from Fig. 2(a) and Fig. 3 that the magnetic properties of the multi-orbital Hamiltonian in the block-OSMP are very accurately reproduced by the generalized Kondo-Heisenberg model. Furthermore, the effective Hamiltonian properly describes other magnetic phases of the OSMP, such as the FM state at $U \gg W$ [16]. However, we remark that Eq. (2) is valid *only* in the OSMP regime. For $U \rightarrow 0$ both orbitals of the multi-orbital system have metallic character, the magnetic moments are not fully developed (Fig. 1), and the system is in a paramagnetic (PM) phase. A detailed U -analysis, Fig. 3(a-e), yields agreement between the models for $U/W \gtrsim 0.5$.

For $U = 0$ (and $K = 0$) the effective Hamiltonian has the form of the widely-studied Kondo-Heisenberg (Kondo) model. Within these limits, we can develop an intuitive understanding of the origin of the magnetic blocks [32–34]. At half-filling $n_K = 1$ and for a strong Kondo (Hund) coupling, $J_K \gg K, t_{00}$, the $\gamma = 0$ electrons form local Kondo interorbital triplets with localized spins. Increasing the mobility of the electrons, t_{00} , leads to the famous (long-range) double-exchange FM ordering [35]. On the other hand, when $t_{00} \gg J_K, K$ one can observe (short-range) features in the spin spectrum upon doping at twice the Fermi vector ($2k_F$) of the itinerant orbitals, Fig. 3(a-b). In the OSMP, when $J_K \sim K \sim \mathcal{O}(t_{00})$, the $2k_F$ instability of itinerant orbitals is amplified leading to spin (quasi)-long-range order with maximum at $S(2k_F)$, see Fig. 3(c-d). As a consequence, competition of double- and super-exchange mechanisms

leads to the formation of block magnetic islands. We test the above “ $2k_F$ prediction” of the maximum of the spin structure factor by comparing q_{\max}^S with the 1D result in the $U \rightarrow 0$ limit, i.e., $2k_F^0 = \pi n_0$. Also, we calculated the Fermi vector position directly from the momentum distribution function $n_\gamma(q)$ via the maximum q_{der}^0 of $dn_0(q)/dq$ (see Fig. 1(e) and [16]). It is evident from the results in Fig. 1(c) that the block-magnetism follows the Fermi vector of the $\gamma = 0$ orbital [36].

As discussed above, the effective Hamiltonian Eq. (2) accurately describes the OSMF magnetic phases, which are in good agreement with the rich island-physics of Kondo-lattice Hamiltonians unveiled before [32, 39–42]. This allows us to create a detailed magnetic phase diagram of the effective model. In Fig. 2(b) we present the n - U dependence of q_{\max}^S using $L = 48$ sites: (i) at $U < W/2$, in the region where the mapping should not work, the system is in a paramagnetic (PM) state; (ii) at $n > 2.5$ and $U > W$ the system is ferromagnetic; (iii) at $n < 2.5$ for all considered U s we have found the novel stable blocks of various sizes, depending on $k_F \propto n$; (iv) finally at $U \gg W$ (not shown) the system is in a FM state for all $2 < n < 3$ [see also Fig. 3(e)]. Furthermore, in between the FM and block phases we have observed incommensurate magnetism around $n \sim 2.5$ (quarter filling $n_K \sim 0.5$ in the Kondo description). This exotic narrow region will be studied in future efforts.

Ladder geometry. To bring our results closer to the experimentally relevant compounds of the AFe_2X_3 family [6–8, 37, 38, 43–45] we will now consider two-orbital ladder systems. The kinetic part of the Hamiltonian is defined with isotropic hoppings $t_{\gamma\gamma'}^\parallel = t_{\gamma\gamma'}^\perp = t_{\gamma\gamma'}$ and $\Delta = 1.6\text{ eV}$ (kinetic energy bandwidth $W_L = 3.55\text{ eV}$), while the remaining interacting portion is the same as in Eq. (1). Figure 4(a) presents the bonding $q_\perp = 0$ component of the spin structure factor $S(q_\parallel, 0)$ for $U = W_L$. Consistent with the 1D predictions, the maximum of $S(q_\parallel, 0)$ strongly depends on filling. At $n = 2.5$ the system is in a π -AFM state, and with increasing filling the spin blocks start to develop. Interestingly, our results indicate that in the $n \rightarrow 2.5$ limit the legs are FM aligned, while in $n \rightarrow 3$ we find a novel AFM ordering between the legs and FM islands involving three spins [46]. The latter may arise from the competition between double-exchange FM ordering and AFM tendencies coming from the localized spins and Fermi instability k_F , i.e., the energy of the large FM blocks as $n \rightarrow 3$ is reduced by the AFM arrangement on the rung. Thus, we speculate that the ladder geometry can stabilize even larger magnetic blocks due to the AFM ordering between the legs.

Consider now the filling dependence of the maximum of the spin structure factor $q_{\max}^{S\parallel}$ for the ladder system. Similarly to the 1D result, $q_{\max}^{S\parallel}$ follows the Fermi vector q_{der}^0 as calculated from the momentum distribution function [see Fig. 4(b)]. However, the filling region where the

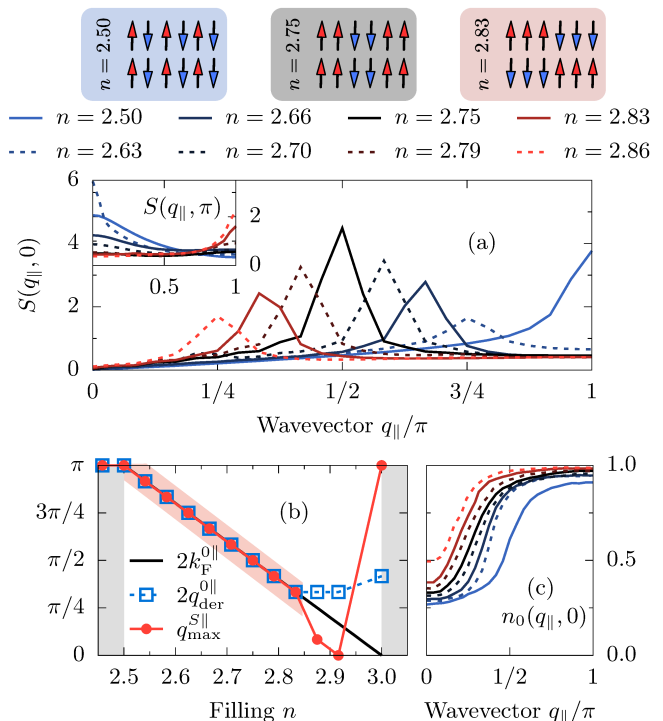


Figure 4. (Color online) (a) Filling n dependence of the bonding component of the spin structure factor $S(q_\parallel, 0)$ as calculated using the two-orbital Hubbard ladder for interaction $U = W_L$ and $L = 48$ sites (24 rungs). The inset depicts the antibonding component $S(q_\parallel, \pi)$. Schematics of the spin configurations are also presented. (b) Filling n dependence of $q_{\max}^{S\parallel}$, $2k_F^{0\parallel} = 2\pi n_0$, and $2q_{\text{der}}^{0\parallel}$. Block-OSMP is indicated as a colored area. (c) Momentum distribution function $n_0(q_\parallel, 0)$ of the $\gamma = 0$ orbital in the bonding $q_\perp = 0$ sector. The legend is the same as for panel (a).

block magnetism is observed, $2.5 < n < 3$, is smaller in comparison to the chain geometry. This dichotomy can be explained by considering the $U \rightarrow 0$ limit prediction of Fermi vectors of the ladder. In this case, for an isotropic ladder ($t_{00}^\parallel = t_{00}^\perp$) for filling $n > 1.5 + 1$, the itinerant orbital Fermi vector is given by $2k_F^{0\parallel} = 2\pi n_0$ (as opposed to $2k_F^0 = \pi n_0$ for a chain geometry). Our results in Fig. 4(b,c) indicate a perfect agreement between $2k_F^{0\parallel}$ and the numerically evaluated $2q_{\text{der}}^{0\parallel}$ [maximum of $dn(q_\parallel, 0)/dq$] in the OSMF. Furthermore, as in the 1D chain, the block-magnetism follows the $2k_F^{0\parallel}$ prediction.

Conclusions. We have shown that the multi-orbital Hubbard model in the OSMF regime can support spin-block magnetism (AFM coupled FM islands) of various novel sizes and shapes, depending on filling and lattice geometry. Moreover, we also derived the effective Hamiltonian of the OSMF, the generalized Kondo-Heisenberg model, which describes all magnetic phases with good accuracy. The observed spin structures are related to the $2k_F$ of the metallic electron bands, but spin blocks are

much more sharply defined than they would be in a mere sinusoidal structure [see real-space spin correlations at the top of Fig. 2(a)], as a weak-coupling Fermi-surface instability would suggest. We believe that the very strongly correlated nature of the localized spins, due to its narrow bandwidth [19], enhances the $2k_F$ instability in a manner only possible in OSMP regimes. All our predictions are relevant for the 123 families of iron-based materials and can be confirmed by INS experiments.

We thank C. Batista and N. Kaushal for fruitful discussions. J. Herbrych, N. D. Patel, A. Moreo, and E. Dagotto were supported by the US Department of Energy (DOE), Office of Science, Basic Energy Sciences (BES), Materials Sciences and Engineering Division. The work of G. Alvarez was conducted at the Center for Nanophase Materials Science, sponsored by the Scientific User Facilities Division, BES, DOE, under contract with UT-Battelle. J. Heverhagen and M. Daghofer were supported by the Deutsche Forschungsgemeinschaft, via the Emmy-Noether program (DA 1235/1-1) and FOR1807 (DA 1235/5-1) and by the state of Baden-Württemberg through bwHPC.

-
- [1] G. R. Stewart, *Rev. Mod. Phys.* **83**, 1589 (2011).
- [2] E. Dagotto, *Rev. Mod. Phys.* **85**, 849 (2013).
- [3] P. Dai, *Rev. Mod. Phys.* **87**, 855 (2015).
- [4] R. M. Fernandes and A. V. Chubukov, *Reports on Progress in Physics* **80**, 014503 (2017).
- [5] A. Georges, L. d. Medici, and J. Mravlje, *Annu. Rev. Condens. Matter Phys.* **4**, 137 (2013), and references therein.
- [6] J. M. Caron, J. R. Neilson, D. C. Miller, K. Arpino, A. Llobet, and T. M. McQueen, *Phys. Rev. B* **85**, 180405 (2012).
- [7] S. Dong, J.-M. Liu, and E. Dagotto, *Phys. Rev. Lett.* **113**, 187204 (2014).
- [8] M. Mourigal, S. Wu, M. B. Stone, J. R. Neilson, J. M. Caron, T. M. McQueen, and C. L. Broholm, *Phys. Rev. Lett.* **115**, 047401 (2015).
- [9] J. Rincón, A. Moreo, G. Alvarez, and E. Dagotto, *Phys. Rev. Lett.* **112**, 106405 (2014).
- [10] J. Herbrych, N. Kaushal, A. Nocera, G. Alvarez, A. Moreo, and E. Dagotto, *Nat. Comm.* **9**, 3736 (2018).
- [11] M. Wang, C. Fang, D.-X. Yao, G. Tan, L. W. Harriger, Y. Song, T. Netherton, C. Zhang, M. Wang, M. B. Stone, W. Tian, J. Hu, and P. Dai, *Nat. Comm.* **2**, 580 (2011).
- [12] B. Wei, H. Qing-Zhen, C. Gen-Fu, M. A. Green, W. Duming, H. Jun-Bao, and Q. Yi-Ming, *Chin. Phys. Lett.* **28**, 086104 (2011).
- [13] Y.-Z. You, H. Yao, and D.-H. Lee, *Phys. Rev. B* **84**, 020406(R) (2011).
- [14] R. Yu, P. Goswami, and Q. Si, *Phys. Rev. B* **84**, 094451 (2011).
- [15] R. Yu and Q. Si, *Phys. Rev. Lett.* **110**, 146402 (2013).
- [16] See Supplementary Material for: (i) analysis of the OSMP, (ii) additional results for the spin structure factor $S(q)$, (iii) details of the mapping to the generalized Kondo-Heisenberg model, and (iv) additional results for the momentum distribution function $n_\gamma(q)$.
- [17] Z. P. Yin, K. Haule, and G. Kotliar, *Nat. Mat.* **10**, 932 (2010).
- [18] P. Dai, J. Hu, and E. Dagotto, *Nat. Phys.* **8**, 709 (2012).
- [19] S. Li, N. Kaushal, Y. Wang, Y. Tang, G. Alvarez, A. Nocera, T. A. Maier, E. Dagotto, and S. Johnston, *Phys. Rev. B* **94**, 235126 (2016).
- [20] N. Kaushal, J. Herbrych, A. Nocera, G. Alvarez, A. Moreo, F. A. Reboredo, and E. Dagotto, *Phys. Rev. B* **96**, 155111 (2017).
- [21] N. D. Patel, A. Nocera, G. Alvarez, A. Moreo, S. Johnston, and E. Dagotto, *arXiv:1807.10419* (2018).
- [22] J. Rincón, A. Moreo, G. Alvarez, and E. Dagotto, *Phys. Rev. B* **90**, 241105(R) (2014).
- [23] S. R. White, *Phys. Rev. Lett.* **69**, 2863 (1992).
- [24] S. R. White, *Phys. Rev. B* **48**, 10345 (1993).
- [25] U. Schollwöck, *Rev. Mod. Phys.* **77**, 259 (2005).
- [26] G. Alvarez, *Comput. Phys. Commun.* **180**, 1572 (2009).
- [27] More technical details about these calculations can be found at [g1257.github.io/papers/88](https://github.com/g1257/papers/88).
- [28] We use standard standard open boundary conditions definitions of the wave-vectors $q = \pi k / (L + 1)$ with $k = 1, \dots, L$.
- [29] Note that in this doping region the orbital $\gamma = 0$ is in a band-insulator state, while the electrons on the $\gamma = 1$ orbital are itinerant ($\delta n_1^2 > 0$).
- [30] On the other hand, patterns with $q_{\max}^S \rightarrow \pi/L$ ($n \rightarrow 3 - 1/L$) are not possible since this would lead (in the extreme) to nonphysical cases involving just one domain wall in the system (spin block of $L/2$ spins).
- [31] J. R. Schrieffer and P. A. Wolff, *Phys. Rev.* **149**, 491 (1966).
- [32] C. D. Batista, J. M. Eroles, M. Avignon, and B. Alascio, *Phys. Rev. B* **58**, R14 689 (1998).
- [33] D. J. Garcia, K. Hallberg, C. D. Batista, M. Avignon, and B. Alascio, *Phys. Rev. Lett.* **85**, 3720 (2000).
- [34] S. Biermann, L. de Medici, and A. Georges, *Phys. Rev. Lett.* **95**, 206401 (2005).
- [35] E. Dagotto, T. Hotta, and A. Moreo, *Physics Reports* **344**, 1 (2001), and references therein.
- [36] It is also interesting to note that $k_F^0 \neq q_{\text{der}}^0$ for the same filling $n \gtrsim 2.7$ for which we observe the breakdown of the magnetic blocks.
- [37] J. M. Caron, J. R. Neilson, D. C. Miller, A. Llobet, and T. M. McQueen, *Phys. Rev. B* **84**, 180409(R) (2011).
- [38] Y. Nambu, K. Ohgushi, S. Suzuki, F. Du, M. Avdeev, Y. Uwatoko, K. Munakata, H. Fukazawa, S. Chi, Y. Ueda, and T. J. Sato, *Phys. Rev. B* **85**, 064413 (2012).
- [39] H. Aliaga, B. Normand, K. Hallberg, M. Avignon, and B. Alascio, *Phys. Rev. B* **64**, 024422 (2001).
- [40] J. C. Xavier, E. Novais, and E. Miranda, *Phys. Rev. B* **65**, 214406 (2002).
- [41] D. J. Garcia, K. Hallberg, C. D. Batista, S. Capponi, D. Poilblanc, M. Avignon, and B. Alascio, *Phys. Rev. B* **65**, 134444 (2002).
- [42] D. J. Garcia, K. Hallberg, B. Alascio, and M. Avignon, *Phys. Rev. Lett.* **93**, 177204 (2004).
- [43] T. Hawai, Y. Nambu, K. Ohgushi, F. Du, Y. Hirata, M. Avdeev, Y. Uwatoko, Y. Sekine, H. Fukazawa, J. Ma, S. Chi, Y. Ueda, H. Yoshizawa, and T. J. Sato, *Phys. Rev. B* **91**, 184416 (2015).
- [44] S. Chi, Y. Uwatoko, H. Cao, Y. Hirata, K. Hashizume, T. Aoyama, and K. Ohgushi, *Phys. Rev. Lett.* **117**, 047003

- (2016).
- [45] M. Wang, S. J. Jin, Ming Yi, Yu Song, H. C. Jiang, W. L. Zhang, H. L. Sun, H. Q. Luo, A. D. Christianson, E. Bourret-Courchesne, D. H. Lee, Dao-Xin Yao, and R. J. Birgeneau, *Phys. Rev. B* **95**, 060502(R) (2017).
- [46] See also D.R. Neuber, M. Daghofer, A.M. Oleś, and W. von der Linden, *physica status solidi (c)*, **3**, 32 (2006).

SUPPLEMENTARY INFORMATION for:

Novel Magnetic Block States in Low-Dimensional Iron-Based Superconductors

by J. Herbrych, J. Heverhagen, N. Patel, G. Alvarez, M. Daghofer, A. Moreo, and E. Dagotto

CONTENTS

S1. Analysis of the OSMP	S1
Charge fluctuations	S1
Density of states	S1
S2. Additional results for the spin structure factor	S2
Finite-size scaling	S2
Results with finite interorbital hybridization	S2
Results for three-orbital Hubbard model	S2
S3. Mapping to the generalized Kondo-Heisenberg model	S3
S4. Additional results for the momentum distribution function	S4

S1. Analysis of the OSMP

Charge fluctuations

Figure S1 shows the interaction U and filling n dependence of the orbital γ resolved charge fluctuations

$$\delta n_\gamma^2 = \langle n_\gamma^2 \rangle - \langle n_\gamma \rangle^2, \quad (\text{S1})$$

together with other single-site expectation values presented already in the main text. Consistent with the OSMP, we find vanishing δn_1^2 when $n_1 = 1$. Simultaneously, $\delta n_0^2 \neq 0$ indicating the itinerant (metallic) character of the $\gamma = 0$ orbital.

Density of states

To strengthen our analysis of the orbital selective Mott phase (OSMP), in Fig. S2 we present the orbital-resolved density of states (DOS) for filling $n = 2.5$ calculated as

$$N_\gamma(\omega) = -\frac{1}{\pi} \sum_k \text{Im} G_\gamma(k, \omega), \quad (\text{S2})$$

where $G(k, \omega)$ is a single-particle Green's function of the γ orbital electrons.

Let us start our analysis of the DOS with the $\gamma = 1$ orbital, Fig. S2(b). Consistent with Mott insulator behavior, upon increasing the interaction U one can observe two Hubbard bands already at $U_c \simeq W/2$, with no states at the Fermi level ϵ_F . For this value of the interaction

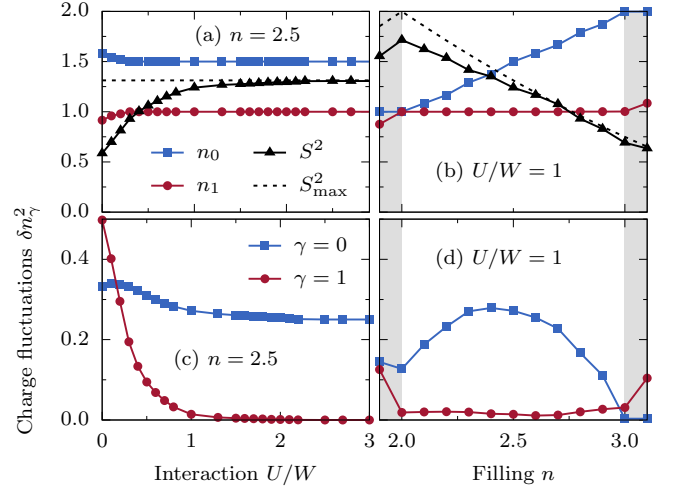


Figure S1. (Color online) (a,c) Interaction U and (b,d) filling n dependence of the total magnetic moment per site $\langle S^2 \rangle$, orbital-resolved occupation numbers n_γ , and charge fluctuations δn_γ^2 of the two-orbital Hubbard model Eq. 1 of the main text, calculated using $L = 48$ sites. In (a,c) $n = 2.5$ and in (b,d) $U = W$. The black dashed lines represent the largest possible magnetic moment S_{\max}^2 .

note that the $\gamma = 1$ orbital is already singly-occupied and that the effective interaction (corresponding to a single-band picture) is $U_c/t_{11} \simeq 7$. As a consequence, the $\gamma = 1$ orbital behaves like a Mott insulator. On the other hand, the $\gamma = 0$ orbital has a nonzero Fermi-level DOS, $N(\epsilon_F) \neq 0$ (or, due to small finite-size effects,

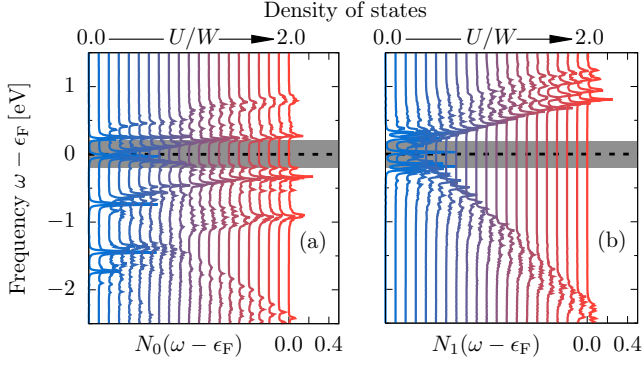


Figure S2. (Color online) Interaction dependence of the orbital-resolved density of states $N_\gamma(\omega)$. Results for (a) $\gamma = 0$ and (b) $\gamma = 1$ calculated for filling $n = 2.5$ and system size $L = 8$ using Lanczos diagonalization (periodic boundary conditions were used). The shaded areas represent π/L estimates of finite-size effects.

in the vicinity of ϵ_F), for all presented values of U , see Fig. S2(a). Such a behavior is consistent with itinerant electrons on orbital $\gamma = 0$ and with the metallic character of this orbital.

S2. Additional results for the spin structure factor

Finite-size scaling

Figure S3(a) presents the finite-size scaling of the maximum of the spin structure factor $S(q_{\max}^S)$ for various doping and interaction U values. Consistent with the discussion presented in the main text, all block-magnetic phases of OSMP manifest a quasi-long range magnetic order, i.e., $U = W$ block-islands for $n = 2.3, 2.5$, and 2.7 . For consistency, we present also results for π -AFM order ($U/W = 1, n = 2$), FM-order ($U/W = 4, n = 2.5$), and paramagnetic (PM) short-range order for $U/W = 0.5, n = 2.5$.

Furthermore, Fig. S3(b) shows the finite-size scaling of the position of the maximum q_{\max}^S . It is evident from the presented results that our block states are not an artifact of finite-size systems: there are well-defined values in the $L \rightarrow \infty$ limit given by πn_0 (arrows).

Results with finite interorbital hybridization

Figure S4 presents results obtained for the two-orbital Hubbard model described in the main text with a finite interorbital hybridization $t_{01} = 0.1$ (the kinetic energy bandwidth is now $W_{\text{OH}} = 2.28$). It is clear that a finite t_{01} does not change the main features of the spin structure factor $S(q)$ (as compared with Fig. 2(a) and Fig. 3(a) of the main text).

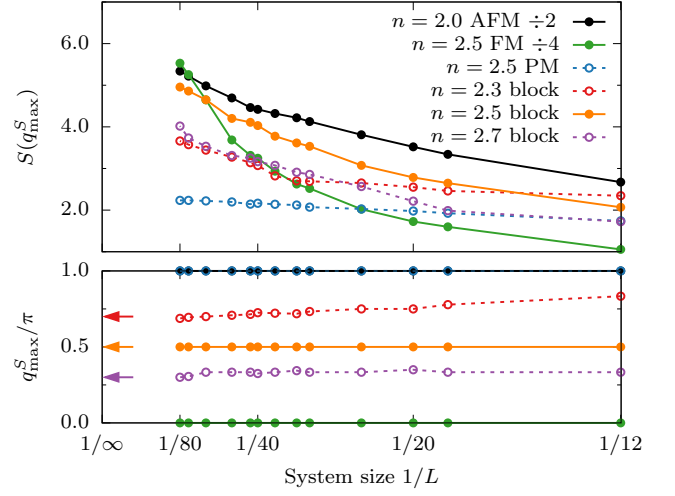


Figure S3. (Color online) Finite-size scaling of (a) the maximum of the spin structure factor $S(q_{\max}^S)$ and (b) position of q_{\max}^S . The presented results are: π -AFM for $n = 2, U/W = 1$; magnetic-block states for $n = 2.3, 2.5, 2.7$ and $U/W = 1$; FM-state for $n = 2.5, U/W = 4$; paramagnetic (PM) state for $n = 2.5, U/W = 0.5$. Arrows in panel (b) represent the $L \rightarrow \infty$ limit given by πn_0 .

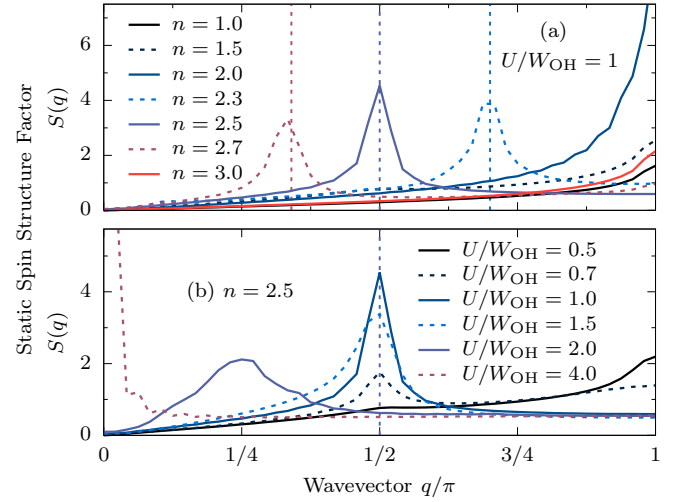


Figure S4. (Color online) Total static structure factor $S(q)$ for (a) various fillings n and fixed values of interaction $U = W_{\text{OH}}$ and (b) for various strengths of interaction U and fixed filling $n = 2.5$, as calculated using $L = 48$ sites and a two-orbital Hubbard model with a finite value of the interorbital hybridization $t_{01} = 0.1$. Dashed vertical lines indicate the value of $2k_F^0 = \pi n_0$.

Results for three-orbital Hubbard model

Figure S5 displays results for $S(q)$ as calculated for the three-orbital Hubbard model. The used parameters are: $t_{00} = t_{11} = -0.5, t_{22} = -0.15, t_{01} = t_{02} = 0.1, \Delta_0 = -0.1, \Delta_1 = 0$, and $\Delta_0 = 0.8$, all in units of

eV. The kinetic energy bandwidth is $W_{3\text{O}} = 2.45\text{ eV}$. Panel (a), (b), and (c) of Fig. S5 depict results for $U/W_{3\text{O}} = 0.6, 0.8, \text{ and } 1.0$, respectively.

In the three-orbital system, $\gamma = 2$ is localized while orbitals $\gamma = 0$ and $\gamma = 1$ are itinerant. As a consequence, the Fermi vector related to the maximum of the spin structure factor can be calculated as $2\bar{k}_F^{-1} = \pi(n_0 + n_1)/2$.

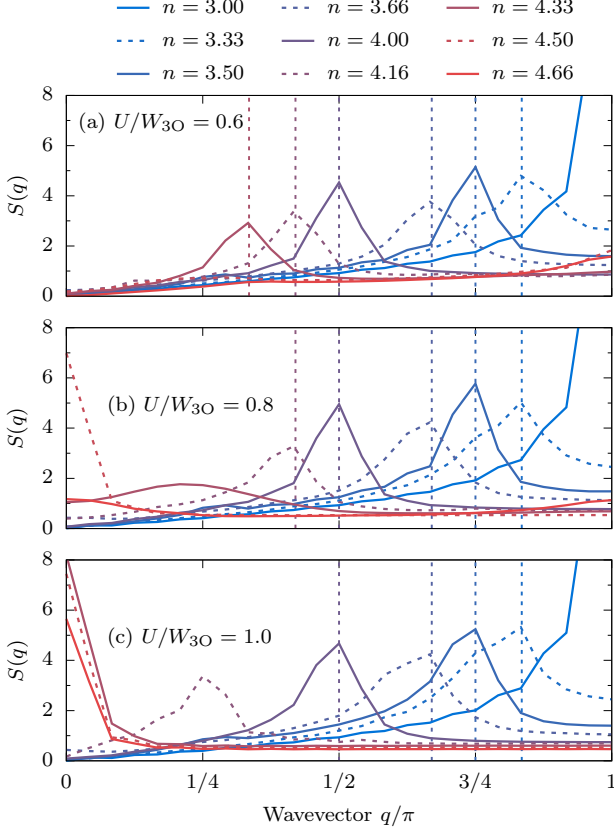


Figure S5. (Color online) Total static structure factor $S(q)$ for various fillings n for the three-orbital Hubbard model as calculated using $L = 24$ sites and interaction (a) $U/W_{\text{OH}} = 0.6$, (b) $U/W_{\text{OH}} = 0.8$, and (c) $U/W_{\text{OH}} = 1.0$. Dashed vertical lines indicate the value of $2\bar{k}_F^{-1} = \pi(n_0 + n_1)/2$.

S3. Mapping to the generalized Kondo-Heisenberg model

Our aim in this section is to find a unitary operator \mathcal{S} via a Schrieffer-Wolff transformation $H_S = e^{i\mathcal{S}}H_{\text{H}}e^{-i\mathcal{S}}$ such that, at a given order, eliminates transitions between states with a different number of doubly occupied sites for the localized orbital $\gamma = 1$. Next, because in the OSMP the states with empty and double occupied sites of the $\gamma = 1$ orbital are highly suppressed [see Fig. 1(e,f) of the main text], we can restrict the Hilbert space of H_S to the subspace with (strictly) one electron per site at this

orbital. In other words, we search for the Hamiltonian

$$H_S = H_{\text{H}} + i[\mathcal{S}, H_{\text{H}}] + \mathcal{O}(\mathcal{S}^2) \quad (\text{S3})$$

for which $N_1 = \sum n_{1,\ell}$ is a good quantum number up to second order in \mathcal{S} , $[H_S, N_1] = \mathcal{O}(\mathcal{S}^2)$, and $N_1^d = \sum n_{1,\ell}^d = \mathcal{O}(\mathcal{S}^2)$ with $n_{\gamma,\ell}^d$ as a doublon number operator.

Let us start by rewriting the two-orbital Hubbard model [Eq. (1) of the main text] in the following form: $H_{\text{H}} = H_0 + H_1 + H_{\text{mix}}$. Here, H_{γ} is the portion of the Hamiltonian which contains the terms solely related to the orbital γ (terms similar to single-band Hubbard Hamiltonian). The H_{mix} part contains the terms which mix the orbitals, i.e., the interorbital interaction $U' = U - 5J_{\text{H}}/2$, Hund coupling, pair-hopping, and the kinetic term containing the orbital hybridization t_{01} . However, only the last two terms can change the doublon number in $\gamma = 1$. Because (i) we neglected the hybridization term, $t_{01} = 0$, and (ii) in the OSMP phase the double occupancy in the $\gamma = 1$ orbital is suppressed and the pair-hopping have negligible contribution, we can assume $[H_{\text{mix}}, N_1] \simeq 0$.

In the rest, consider H_1 as

$$H_1 = t_{11}H_1^0 + t_{11}H_1^+ + t_{11}H_1^- + UH_1^U, \quad (\text{S4})$$

where H_1^0 contains the terms that do not change the double occupancy in the $\gamma = 1$ orbital (hopping of the holes and doublons), H_1^+ (H_1^-) contains the terms which increase (decrease) the doublon number on the $\gamma = 1$ orbital, and H_1^U which is the Hubbard- U term on the $\gamma = 1$ orbital. It can be shown that

$$\begin{aligned} H_1^+ &= - \sum_{\ell,\sigma} \left[n_{1,\ell,-\sigma} c_{1,\ell,\sigma}^\dagger c_{1,\ell+1,\sigma} \tilde{n}_{1,\ell+1,-\sigma} + \text{H.c.} \right], \\ H_1^0 &= - \sum_{\ell,\sigma} \left[n_{1,\ell,-\sigma} c_{1,\ell,\sigma}^\dagger c_{1,\ell+1,\sigma} n_{1,\ell+1,-\sigma} \right. \\ &\quad \left. + \tilde{n}_{1,\ell,-\sigma} c_{1,\ell,\sigma}^\dagger c_{1,\ell+1,\sigma} \tilde{n}_{1,\ell+1,-\sigma} + \text{H.c.} \right], \end{aligned} \quad (\text{S5})$$

where $\tilde{n}_{1,\ell,\sigma} = (1 - n_{1,\ell,\sigma})$ and also $H_1^- = (H_1^+)^\dagger$. Collecting the terms in Eq. (S3) we obtain

$$\begin{aligned} H_S &= H_0 + H_{\text{mix}} + t_{11}H_1^0 + t_{11}H_1^+ + t_{11}H_1^- + UH_1^U \\ &\quad + i[\mathcal{S}, H_{\text{H}}] + \mathcal{O}(\mathcal{S}^2). \end{aligned} \quad (\text{S6})$$

In order to eliminate the transitions between the states with different doublon number on the $\gamma = 1$ orbital we have to require the $i[\mathcal{S}, H_{\text{H}}]$ term to eliminate the H_1^\pm contribution. The latter can be achieved via

$$\mathcal{S} = -i \frac{t_{11}}{U} (H_1^+ - H_1^-), \quad (\text{S7})$$

and as a consequence $\mathcal{O}(\mathcal{S}^2) \propto t_{11}^3/U^2$. For the system parameters considered in Eq.(1) $t_{11}^3/U^2 \ll W$ in the OSMP.

In the last step we have to evaluate $[\mathcal{S}, H_{\text{H}}]$. Some observations are in order:

- (i) $[\mathcal{S}, H_0] = 0$, since the operator \mathcal{S} contains only the terms involving $\gamma = 1$.
- (ii) It can be shown that $iU[\mathcal{S}, H_1^U] = -(H_1^+ + H_1^-)$. Note that this contribution removes (as required) transitions between different doubly occupied sites at the $\gamma = 1$ orbital.
- (iii) The term $[\mathcal{S}, H_1^0]$ will involve a single occurrence of the H_1^\pm operator and, therefore, it will be increasing/decreasing the double occupancy at $\gamma = 1$. Since the latter is not allowed in our restricted space, this term can be omitted.
- (iv) At half-filling, $n_1 = 1$, H_1^0 can be also neglected since it describes the hopping of doublons and holons, not present in OSMP.
- (v) In the restricted subspace of one electron per site at the $\gamma = 1$ orbital the H_1^U term, together with the U' and pair-hopping term in H_{mix} , can be dropped. The first two are just constants, where the last one is strictly 0.
- (vi) Also, the term proportional to $H_1^+ H_1^-$ can be omitted, since it creates (at half-filling) a holon-doublon pair not allowed in the reduced Hilbert space.
- (vii) The term $[\mathcal{S}, H_{\text{mix}}]$ will contain terms which conserves doublons (H_{mix}) and terms which change the doublon number (\mathcal{S}). As a consequence, similarly to the point (iii), this contribution can be omitted in our restricted space.
- (viii) The term $-t_{11}^2/UH_1^-H_1^+$ can be written as $4t_{11}^2/U \sum_{\ell} \mathbf{S}_{1,\ell} \cdot \mathbf{S}_{1,\ell+1}$ (virtual spin flips) where $\mathbf{S}_{1,\ell}$ is the total spin at site ℓ of orbital $\gamma = 1$.

An attentive reader will recognize that, due to the assumptions justified when addressing the OSMP regime, the above transformation is simply a “large- U ” Hubbard to Heisenberg mapping involving the localized $\gamma = 1$ orbital. Collecting relevant terms, and omitting the $\mathcal{O}(t_{11}^2/U)$ term, the above Hamiltonian can be written in the familiar form of the generalized Kondo-Heisenberg model, namely

$$H_K = t_{00} \sum_{\ell,\sigma} \left(c_{0,\ell,\sigma}^\dagger c_{0,\ell+1,\sigma} + \text{H.c.} \right) + U \sum_{\ell} n_{0,\ell,\uparrow} n_{0,\ell,\downarrow} - J_K \sum_{\ell} \mathbf{S}_{0,\ell} \cdot \mathbf{S}_{1,\ell} + K \sum_{\ell} \mathbf{S}_{1,\ell} \cdot \mathbf{S}_{1,\ell+1}, \quad (\text{S8})$$

with $K = 4t_{11}^2/U$ and $J_K = 2J_H$.

S4. Additional results for the momentum distribution function

Figure S6 presents an analysis of the momentum distribution function

$$n_\gamma(q) = \sum_{\ell,\kappa,\sigma} e^{iq(\ell-\kappa)} \langle c_{\gamma,\ell,\sigma}^\dagger c_{\gamma,\kappa,\sigma} \rangle. \quad (\text{S9})$$

In panels (a-d), we show the interaction U and filling n dependence of $n_\gamma(q)$. Furthermore, in Fig. S6(e) we present the comparison between the two-orbital and generalized Kondo-Heisenberg model of $2q_{\text{der}}^0$ maximum. Similarly to the case of the spin structure factor $S(q)$, we have found a perfect agreement for $U/W \gtrsim 0.5$.

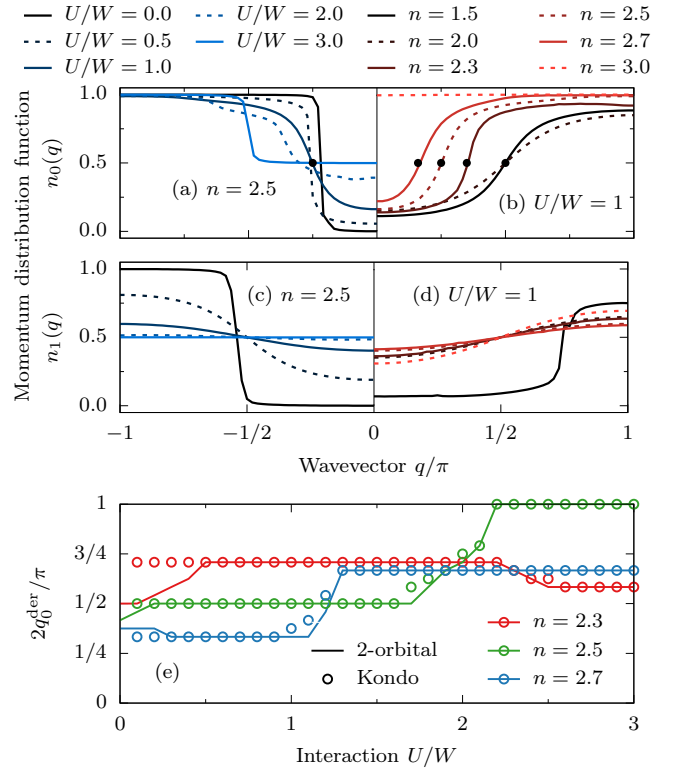


Figure S6. (Color online) (a,c) Interaction U and (b,d) filling n dependence of the orbital-resolved momentum distribution function $n_\gamma(q)$ of the two-orbital Hubbard model (using $L = 48$ sites). The upper (lower) row represents results for $\gamma = 0$ ($\gamma = 1$). Black points depict the position of the maximum of the derivative $dn_0(q)/dq$, i.e., q_{der}^0 . (e) Interaction dependence of $2q_{\text{der}}^0$. Lines (points) represent results obtained with a two-orbital Hubbard model (generalized Kondo-Heisenberg model).